BI-3406, a potent and selective SOS1::KRAS interaction inhibitor, is effective in KRAS-driven cancers through combined MEK inhibition

Marco H. Hofmann[#1], **Michael Gmachl**[#1], **Juergen Ramharter**[#1], **Fabio Savarese**[1], **Daniel Gerlach**[1], **Joseph R. Marszalek**[3], **Michael P. Sanderson**[1], **Dirk Kessler**[1], **Francesca Trapani**[1], **Heribert Arnhof**[1], **Klaus Rumpel**[1], **Dana-Adriana Botesteanu**[1], **Peter Ettmayer**[1], **Thomas Gerstberger**[1], **Christiane Kofink**[1], **Tobias Wunberg**[1], **Andreas Zoephel**[1], **Szu-Chin Fu**[4], **Jessica L. Teh**[3], **Jark Böttcher**[1], **Nikolai Pototschnig**[1], **Franziska Schachinger**[1], **Katharina Schipany**[1], **Simone Lieb**[1], **Christopher P. Vellano**[3], **Jonathan C. O'Connell**[2], **Rachel L. Mendes**[2], **Jurgen Moll**[1], **Mark Petronczki**[1], **Timothy P. Heffernan**[3], **Mark Pearson**[1], **Darryl B. McConnell**[1], **Norbert Kraut**[1]

[1]Boehringer Ingelheim RCV GmbH & Co KG, Vienna, Austria

[2]Forma Therapeutics, Watertown, MA, USA

[3]TRACTION Platform, Therapeutics Discovery Division, The University of Texas MD Anderson Cancer Center, Houston, TX 77030, USA

[4]Department of Genomic Medicine, The University of Texas MD Anderson Cancer Center, Houston, TX 77030, USA

[#] These authors contributed equally to this work.

Abstract

KRAS is the most frequently mutated driver of pancreatic, colorectal, and non-small cell lung cancers. Direct KRAS blockade has proven challenging and inhibition of a key downstream effector pathway, the RAF-MEK-ERK cascade, has shown limited success due to activation of feedback networks that keep the pathway in check. We hypothesized that inhibiting SOS1, a KRAS activator and important feedback node, represents an effective approach to treat KRAS-driven cancers. We report the discovery of a highly potent, selective and orally bioavailable small-

Corresponding Authors: Marco H. Hofmann, marco.hofmann@boehringer-ingelheim.com and Norbert Kraut, norbert.kraut@boehringer-ingelheim.com, Boehringer Ingelheim RCV GmbH & Co KG, Dr. Boehringer-Gasse 5-11, A-1121 Vienna, Austria, Tel. +431 80105-2790.
Michael P. Sanderson is a former employee of Boehringer Ingelheim RCV GmbH & Co KG, Vienna, Austria now working for Merck KGaA. Jurgen Moll is a former employee of Boehringer Ingelheim RCV GmbH & Co KG now working for Sanofi. Rachel L. Mendes is a former employee of Forma Therapeutics now working for PerkinElmer. Jonathan C. O'Connell is a former employee of Forma Therapeutics now working for Integral Health.

molecule SOS1 inhibitor, BI-3406, that binds to the catalytic domain of SOS1 thereby preventing the interaction with KRAS. BI-3406 reduces formation of GTP-loaded RAS and limits cellular proliferation of a broad range of KRAS-driven cancers. Importantly, BI-3406 attenuates feedback reactivation induced by MEK inhibitors and thereby enhances sensitivity of KRAS-dependent cancers to MEK inhibition. Combined SOS1 and MEK inhibition represents a novel and effective therapeutic concept to address KRAS-driven tumors.

Introduction

KRAS functions as a molecular switch, cycling between inactive (GDP-bound) and active (GTP-bound) states to transduce extracellular signals via cell-surface receptors. KRAS signaling occurs through engagement with effector proteins that orchestrate intracellular signaling cascades regulating tumor cell survival and proliferation. Aberrant activation of KRAS by deregulated upstream signaling (1), loss of GTPase-activating protein function (2,3) or oncogenic mutations result in increased GTP-bound KRAS and persistent downstream signaling (4,5). Mutations in the *KRAS* gene occur in approximately 1 out of 7 of all human cancers, making it the most frequently mutated oncogene (6,7). Up to 90% of pancreatic tumors bear activating *KRAS* mutations. Mutated *KRAS* is also observed at high frequency in other common tumors, including colorectal cancer (~44%) and non-small cell lung cancer (~29%). Cancer-associated mutations in KRAS cluster in three hotspots (G12, G13, Q61), with a majority (77%) of mutations causing single amino-acid substitutions at G12. The KRAS missense mutation G12D is the most predominant variant in human malignancies (35%), followed by G12V (29%), G12C (21%), G12A (7%), G12R (5%), and G12S (3%). Besides G12, the hotspots G13 and Q61 show mutation rates of 10% and 6% respectively (*KRAS* mutation frequencies were derived from AACR GENIE v6.1 and TCGA) (6,7). In preclinical models, activated KRAS has been shown to drive both the initiation and maintenance of a range of cancer types (8–11). Despite the compelling rationale to target KRAS, identification of potent direct inhibitors has been challenging. Promising early results from clinical trials with the two inhibitors AMG 510 and MRTX849, both targeting the KRAS G12C mutant allele covalently and specifically (12,13), have been reported. These inhibitors demonstrated clinical activity primarily in non-small cell lung cancer (NSCLC), where the KRAS G12C mutation frequency is highest (14,15). Moreover, a nanomolar pan-RAS inhibitor binding to a second pocket on RAS has been described (16).

Despite this recent success, molecularly targeted therapies that effectively address the most prevalent KRAS mutant alleles beyond G12C, including G12D and G12V, are lacking. Attempts to indirectly target KRAS-driven tumors through inhibition of downstream effectors of KRAS, such as members of the RAF-MEK-ERK cascade, has suffered limited clinical success (17) in part due to the capacity of cancer cells to adapt by rapidly increasing KRAS-GTP levels. The SHP2 protein-tyrosine phosphatase is an important mediator of cellular signaling through the RAS/MAP kinase pathway and is thought to act via activation of SOS1-regulated RAS-GTP loading. SHP2 inhibitors are being explored by several companies with the most advanced inhibitors, RMC-4630 and TN0155, currently under study in phase 1 clinical trials (18–21). Published data show particular sensitivity to SHP2i inhibitors in KRAS G12C mutant tumors (20).

Dynamic control of the extent and kinetics of the RAS-RAF-MEK-ERK signaling is governed by positive and negative feedback loops (22). SOS1 is a key guanine exchange factor (GEF) for KRAS that binds and activates GDP-bound RAS-family proteins at its catalytic binding site and in this way promotes exchange of GDP for GTP. In addition to its catalytic site, SOS1 can also bind GTP-bound KRAS at the allosteric site that potentiates its GEF function, constituting a mechanism for positive feedback regulation (23). Depletion of SOS1 or specific genetic inactivation of its GEF function has been shown to decrease the survival of tumor cells harboring a *KRAS* mutation (24). This effect was not observed in wild-type cells that are not KRAS addicted (24). Pathway activation leads to ERK-mediated phosphorylation of SOS1 but not its paralog SOS2 thereby attenuating of SOS1 GEF activity (25,26). This suggests that SOS1 acts as an important node in the negative feedback regulation of the KRAS pathway (25,26). Based on these lines of evidence, we hypothesized that a potent and selective SOS1 inhibitor would synergize with a MEK inhibitor, resulting in strong and sustained pathway blockade and a robust anti-tumor efficacy in KRAS-driven cancers.

In 2014, small molecules have been described which bind to a lipophilic pocket of SOS1, in close proximity to the RAS binding site (27). Binding of these ligands increased SOS1-mediated nucleotide exchange and consequently led to activation of RAS. Recently, SOS1 inhibitor tool compounds were reported (28), but these non-bioavailable compounds did not demonstrate the expected differential effect on KRAS-driven cancer cell lines versus wild-type cells.

In this paper, we describe the discovery of BI-3406, a potent and selective SOS1::KRAS interaction inhibitor, and elucidate its mode of action both *in vitro* and *in vivo*. BI-3406 potently decreases the formation of GTP-loaded RAS and reduces cell proliferation of a large fraction of KRAS G12C- and non-G12C-driven cancers *in vitro* and *in vivo*. BI-3406 attenuates feedback reactivation by MEK inhibitors and enhances sensitivity of KRAS-dependent cancers to MEK inhibition, resulting in tumor regressions at well-tolerated doses in mouse models. Our data provide strong evidence that combined SOS1 and MEK inhibition represents an attractive therapeutic concept to address KRAS-driven human tumors.

Results

Discovery of BI-3406, a potent and selective SOS1::KRAS interaction inhibitor

To discover SOS1 inhibitors, we conducted a high throughput screen of 1.7 million compounds using an alpha screen and a fluorescence resonance energy transfer assay as an orthogonal biochemical screen on SOS1 and KRAS G12D. Several hits containing a quinazoline core were identified, best exemplified by BI-68BS (Supplementary Fig. S1a). A stoichiometric and saturable dissociation constant, using surface plasmon resonance on SOS1 (K_D = 470 nM) and the corresponding activity in a GDP-dependent KRAS-SOS1 displacement assay (IC_{50} = 1.3 μM), indicated effective disruption of the SOS1-KRAS protein-protein interaction. Co-crystallization of BI-68BS and SOS1 confirmed binding to a pocket (27) next to the catalytic binding site on SOS1 (Supplementary Fig. S1b, S1c and Supplementary Table S1) with the quinazoline ring pi-stacking to His905[SOS1]. Based on the

structural data, the interaction of the methoxy substituent of BI-68BS with Tyr884[SOS1] most likely interferes with the competing Tyr884[SOS1]-Arg73[RAS] interaction and consequently prevents KRAS from binding to SOS1 (Supplementary Fig. S1d). In an effort to optimize BI-68BS, several modifications were made, which led to the discovery of BI-3406 (Fig. 1a). As BI-68BS was originally synthesized as part of a project targeting EGFR, a methyl substituent was incorporated in the 2-position of the quinazoline core to effectively eliminate any interfering inhibition of kinase activity (tested in a panel of 324 kinases, Supplementary Table S2 and S3). Introduction of a trifluoromethyl and an amino substituent at the phenethyl moiety filled the pocket more effectively and formed an H-bond with M878[SOS1] respectively, thereby significantly increasing potency. The tetrahydrofuryl substituent favorably balanced solubility and metabolic stability and improved interaction with Tyr884[SOS1]. Synthesis of BI-3406 is described in detail in the supplementary data section (for synthesis route see also Supplementary Fig. S1e and S1f.). Crystallization data can be found in Supplementary Table S1.

A detailed biochemical characterization of BI-3406 was made possible through the analysis of a variety of interaction assays using SOS1 and SOS2 recombinant proteins, in combination with several KRAS mutant variants. BI-3406 was found to be a potent, single digit nanomolar inhibitor binding to the catalytic site of SOS1 and thereby blocking the interaction with KRAS-GDP, as exemplified in the interaction assay with KRAS G12D and G12C mutant oncoproteins (Fig.1b).

A recently developed covalent KRAS G12C-specific inhibitor (ARS-1620) was able to interfere with the SOS1-KRAS G12C protein-protein interaction but, in contrast to BI-3406, had no effect on the protein-protein interaction of SOS1 with KRAS G12D (Fig. 1c, d). Upon replacing SOS1 with its paralog SOS2, BI-3406 lost its ability to interfere with KRAS binding, indicating that BI-3406 is a highly potent, SOS1 specific inhibitor that can address multiple KRAS mutant oncoproteins (Fig. 1b). The SOS1 selectivity of BI-3406 can be explained by a potential clash of the compound with Val903 and the absence of pi-interaction in SOS2, which is revealed in an overlay of the published SOS2 apo structure (PDB Code 6EIE) with our SOS1 BI-3406 co-crystal structure (Supplementary Fig. S1g). In a biochemical protein-protein interaction assay, the introduction of the mutations Y884A and H905V in a recombinant SOS1 protein strongly impaired the ability of BI-3406 to disrupt the interaction with KRAS G12D (Supplementary Fig. S1h). Importantly, expression of FLAG-SOS1 transgenes in Mia PaCa-2 and HEK293 cells revealed that the SOS1 mutations H905V and H905I abrogated the ability of BI-3406 to inhibit phosphorylation of ERK (pERK) and cell proliferation, demonstrating selective SOS1 on-target activity of the compound in a cellular context. (Fig. 1e, f and Supplementary Fig. S1i).

To further investigate whether BI-3406 was capable of cellular SOS1 inhibition, cells were treated with increasing concentrations of BI-3406. The compound inhibited RAS-GTP levels with an IC50 of 83–231 nM in SOS1/KRAS-dependent NCI-H358 (KRAS G12C) and A549 (KRAS G12S) cells (Fig. 1g). Stimulation of starved NCI-H358 and MIA PaCa-2 cells with EGF resulted in an increase of RAS GTP levels that could be blocked by the addition of BI-3406 (Supplementary Fig. S1j). Based on our mechanistic findings that BI-3406 selectively targets SOS1, we next wanted to address its cellular selectivity profile. As there

are no known substrate differences distinguishing SOS1- and SOS2-mediated effects, we reasoned that a SOS1-selective inhibitor should have an increased impact on cellular signaling in a SOS2-null background. Accordingly, we generated NCI-H358 cells in which SOS2, and for comparison SOS1, was genetically inactivated (Supplementary Fig. S1k) and measured RAS GTP levels after treatment with BI-3406. The effect of BI-3406 on RAS-GTP levels was significantly more pronounced in NCI-H358 cells harboring a SOS2 knockout when compared to the parental cell line (Supplementary Fig. S1l). Moreover, the effect of BI-3406 on pERK levels was enhanced in NCI-H358 SOS2 null cells compared to parental cells, while being strongly reduced in SOS1 knockout cells (Supplementary Fig. S1m). The anti-proliferative effect of BI-3406 was enhanced in SOS2 knockout cells, compared to parental cells (Supplementary Fig. S1n). In SOS1 knockout cells, no effect on proliferation was observed following treatment with BI-3406 (Supplementary Fig. S1n). Analysis of a time-course treatment of NCI-H358 cells (KRAS G12C) with BI-3406 revealed a rapid reduction of RAS-GTP levels that correlated with the effect on pERK levels (Supplementary Fig. S1o). RAS-GTP and pERK returned to levels close to baseline at the 24 hour time point. These data further support the notion that BI-3406 is a potent and SOS1-selective inhibitor.

Association of *KRAS* mutation status with sensitivity to SOS1 inhibition

The cellular activity of BI-3406 was further evaluated across a wider panel of cancer cell lines driven by different KRAS pathway activating mutations. As SOS1 is uniformly expressed across all tumor types, a SOS1 inhibitor could be broadly applicable in KRAS driven indications (Supplementary Fig. S2a and S2b). Plotting the expression of SOS1 against SOS2 revealed that the cell lines used in our subsequent experiments harbored SOS1/SOS2 mRNA ratios representative of ratios observed in a large dataset of human tumors (Supplementary Fig. S2c). A dose-dependent partial reduction of pERK levels was observed in all RAS-mutated cell lines tested, with an IC50 between 17 and 57 nM (IC50 value defined as the inflection point of the curve) (Fig. 2a). No pERK modulation was observed in A375 melanoma cells that are KRAS wild-type and harbor an activating BRAF V600E mutation that likely renders them independent of KRAS signaling (Fig. 2a).

Cell lines expressing mutant *KRAS* have demonstrated variable dependencies upon KRAS for viability in two-dimensional (2D) monolayer proliferation assays (29), while KRAS-dependency is better modelled in anchorage-independent 3D growth assays. Consistent with this observation, we demonstrated that BI-3406 inhibited the 3D growth of 4 *KRAS* mutant cancer cells with a IC50 of 16–52 nM, as half-maximum inhibitory concentration (Fig. 2b). In contrast, the 3D growth of the two KRAS wild-type cancer cell lines, NCI-H520 and A375, was not appreciably affected (Fig. 2b), but responded to the broad anti-proliferative agent panobinostat, an HDAC inhibitor (Fig. 2c). Collectively, these data show a clear correlation between signaling pathway and growth inhibition by BI-3406 in KRAS-driven cancer cell lines.

The growth inhibitory effects of BI-3406 across different *KRAS* mutated cell lines could be influenced by tumor lineage or co-mutations. Therefore, we evaluated the effect of SOS1 inhibition on a panel of isogenic cell lines, differing only in the status of their *KRAS* allele.

We used NCI-H23 cells carrying a heterozygous KRAS G12C allele and replaced the G12C codon by heterozygous G12D, G12V, G12R, G13D or homozygous G12D, G13D and Q61H mutations. BI-3406 showed comparable activity, independent of zygosity, with an approximate 50% reduction of pERK levels in all KRAS variant isogenic cell lines (Fig. 2d). Reduction of pERK correlated with reduced proliferation of NCI-H23 isogenic cell lines, indicating cellular sensitivities of the most prevalent KRAS G12 and G13 oncogenic variants (Fig. 2d, e). Only weak inhibition of pERK levels were observed in cells carrying the Q61H oncogenic variant, that was recently reported to lack intrinsic GTP hydrolysis activity and to exhibit increased affinity for RAF (30). No modulation of pERK was observed in cells carrying the G12R variant (Fig. 2d), a variant that was recently described not to interact with the catalytic domain of SOS1 (31). In a cellular context in which the KRASG12C mutation was reverted to wild-type KRAS, pERK modulation was observed following treatment with BI-3406, but the wild-type cells were no longer able to grow in a 3D proliferation assay.

We further profiled BI-3406 in a larger panel of 40 solid cancer cell lines with known oncogenic alterations in *KRAS*, *NRAS*, *HRAS*, *EGFR*, *NF1,* and *BRAF* (Fig. 2f and Supplementary Table S4 and S5). Excitingly, BI-3406 sensitivity correlated with KRAS mutation status in this larger cell panel (Fisher's exact test, p-value 0.00337) (Fig. 2f). Sensitive cell lines harbored a broad range of *KRAS* mutant alleles (Supplementary Table S4 and S5), including KRAS G12C, G12V, G12S, G12A and G13D mutations. Although no difference in sensitivity could be observed based on the zygosity of the *KRAS* mutation, it was notable that two out of the three non-responsive *KRAS* mutant cell lines, as well as three out of five non-responsive *NRAS* mutant cell lines, were characterized by a Q61 mutation. NF1 is a tumor suppressor and a RAS GTPase-activating protein (GAP) (2). Loss of NF1 function has been shown to increase RAS-GTP levels, hyperactivate RAS/MAPK signaling and contribute to a variety of human cancers (32,33). Therefore, we assessed whether *NF1* aberrations in cell lines resulted in sensitivity to SOS1 inhibition. Interestingly 7 out of 14 cell lines carrying *NF1* aberrations were sensitive to BI-3406 treatment, irrespective of their *KRAS* status. No other driver mutations in components of the RTK/KRAS/MAPK pathway could be identified in several of these sensitive cell lines, suggesting *NF1* aberrations are a key determinant for sensitivity to BI-3406 in these lines (Supplementary Table S4). Similarly, a fraction of NSCLC cell lines driven by *EGFR* mutations also responded to BI-3406 treatment, suggesting that oncogenic RTKs can confer sensitivity to SOS1 inhibition. As none of the six *BRAF* mutant and five *NRAS* mutant cell lines were sensitive to treatment with BI-3406, (Fig. 2f) we hypothesize that *NRAS* and *BRAF* mutations are associated with resistance to BI-3406 monotherapy (p-value < 0.001). Collectively, our findings highlight the critical function of SOS1 in promoting KRAS/MAPK pathway activation in a large fraction of cancers driven by KRAS G12C- and non-G12C alleles, *NF1* aberrations, as well as *EGFR* mutations.

The pharmacodynamics of BI-3406 were further evaluated. In sensitive cell lines, treatment with BI-3406 resulted in sustained pathway modulation of ERK1/2 phosphorylation (Supplementary Fig. S2d and S2e), in contrast to insensitive cell lines, that exhibited weaker and more short-lived effects (NCI-H2170 and NCI-H1299) (Supplementary Fig. S2e). Compared to pERK, levels of pAkt Ser473 and Thr308 were less strongly affected by BI-3406 (Supplementary Fig. S2d and S2e).

We subsequently tested BI-3406 side-by-side with the recently reported SOS1 inhibitor BAY293 (28) and the SHP2 inhibitor SHP099 (18) in 2D and 3D proliferation assays across a panel of 24 cell lines, including 18 KRAS-mutated cell lines (Supplementary Table 6). The three compounds demonstrated no activity in 2D proliferation assays. In 3D proliferation assays, SHP099 showed the strongest anti-proliferative effects with an IC50 between 167–790 nM in KRAS G12C, a subset of G12D cell lines, and in one G12S cell line it yielded modest effects in KRAS G13D and G12V cells (IC50:1180–4411 nM), while no effects were detectable in Q61L/H and G12R KRAS mutant tumor cells. BI-3406 caused cell growth inhibition in all KRAS G12 and G13 mutant cell lines (IC50: 9–220 nM) with the exception of G12R and KRAS Q61L/H mutant tumor cells. The previously published SOS1 inhibitor BAY293 demonstrated only a very limited potency and, in contrast to BI-3406, no sizeable selectivity for KRAS mutated cells, as compared to KRAS wild-type cells (Supplementary Table S6). This suggests that BI-3406 and SHP099 possess a partially overlapping yet distinct profile across KRAS mutated cell lines, with BI-3406 being more broadly active in 3D proliferation assays.

To glean first insights regarding a potential therapeutic index of BI-3406, we tested the compound on primary cells and non-tumorigenic cells *in vitro*. BI-3406 inhibited the proliferation of foreskin fibroblasts with an IC50 of 37 nM, while 2 other cell types, primary smooth muscle cells and retinal pigment epithelial cells, were not impacted (IC50>5μM) (Supplementary Fig. S2f–h). The extremely potent and widely used MEK inhibitor trametinib affected proliferation of all 3 aforementioned cell types (retinal pigment epithelial cells IC50 of 12 nM, primary smooth muscle cells 843 nM, normal foreskin cells IC50 of 85 nM).

SOS1 inhibition suppresses tumor growth in xenograft models of KRAS-driven cancers

BI-3406 is an orally bioavailable compound (Supplementary Fig. S3a) and single administration was sufficient to reduce RAS-GTP and pERK levels in A549 xenograft tumors over a period of 24 hours and 7 hours, respectively (Supplementary Fig. S3b–c). At a dose of 50 mg/kg bid, relevant levels of unbound exposures are achieved for the first 12 hours, when compared to unbound IC50 levels in A549 cells (Supplementary Fig. S3a). In MIA PaCa-2 tumor bearing mice, twice daily compound treatment with 50 mg/kg BI-3406 resulted in pathway modulation over a period of up to 10 hours (Fig. 3a and Supplementary Fig. S3d). At the 24 h time point, the compound was cleared (Supplementary Fig. S3a and S3d) and pERK levels returned to baseline in both A549 and MIA PACa-2 tumors (Fig. 3a and Supplementary Fig. S3b). In the same experiment, a reduction of pERK was observed by immunohistochemistry in surrogate tissue (murine skin) over a similar period (Fig. 3b and Supplementary Fig. S3e). As the use of phosphorylation markers can be challenging in a clinical setting, effects on *RAS* dependent gene expression signatures were analyzed in the MIA PaCa-2 xenograft model. Prolonged suppression of known pathway-related genes, such as *SPRY4*, *DUSP6*, and transcriptional regulators, such as *FOSL1*, *EGR1*, *ETV1*, *ETV4* and *ETV5* was observed (Fig. 3c, Supplementary Fig. S3f and Supplementary Table S7) in line with published data on gene expression responses to other specific MAPK pathway inhibitors (34,35). Of note, no effects on SOS2 mRNA expression were observed upon

treatment with BI-3406 during the period of observation (Supplementary Fig. S3g–h) suggesting no compensatory upregulation.

Based on its potent cellular activity and favorable pharmacokinetic properties, the efficacy of BI-3406 was evaluated in established, subcutaneous KRAS G12C-mutated MIA PaCa-2 xenografts. Twice daily treatment with either 12 or 50 mg/kg of BI-3406 was well tolerated and resulted in a prolonged dose-dependent tumor growth inhibition (p<0.005 as compared to vehicle control, Fig. 3d, 3e). Similar tumor growth inhibitory effects were observed in KRAS G12V-mutated SW620, the KRAS G13D-mutated LoVo and the KRAS G12S-mutated A549 xenograft models (Fig. 3f, Supplementary Fig. S3i and S3j). No anti-tumor response was observed in the BRAF mutant A375 xenograft model (Supplementary Fig. S3k), consistent with the lack of effect on cell proliferation in this cell line *in vitro*. Thus, oral administration of BI-3406 monotherapy inhibits the growth of KRAS G12C, G12V, G13D and G12S mutated xenograft models.

Dual SOS1 and MEK inhibition as effective strategy to treat KRAS-mutant tumors

Previous work showed that many cancer models develop adaptive resistance to MEK inhibitors, often due to the reactivation of SOS1 (17). Therefore, we reasoned that dual SOS1 and MEK inhibition could constitute an effective strategy to treat KRAS mutant tumors. Consistent with this hypothesis, the combination of BI-3406 with the MEK inhibitor trametinib yielded strong synergistic anti-proliferative effects in MIA PaCa-2 (KRAS G12C) and DLD1 (KRAS G13D) cells *in vitro* (Supplementary Fig. S4a). Based on these promising cellular data, we tested BI-3406 plus trametinib in both the pancreatic cancer MIA PaCa-2 and the colorectal LoVo (KRAS G13D) xenograft mouse models. The MEK inhibitor trametinib was primarily used due to its favorable mouse pharmacokinetic properties ($t_{1/2}$ = 33 hours) (36). The combination of 50 mg/kg BI-3406 twice daily with the clinically relevant dose of trametinib (0.1–0.125 mg/kg, bid; for calculations details please see description in Supplementary Data) was well tolerated (Supplementary Fig. S4b and S4c) and caused substantial regressions in the entire cohort of MIA PaCa-2 tumor bearing mice (Fig. 4a and b). Furthermore, following combination treatment, slow regrowth of tumors was detectable only 22 days after drug withdrawal (Fig. 4a). Similar results were observed in LoVo xenografts, with the effect of the BI-3406 and trametinib combination therapy being significantly stronger compared to both monotherapies, with sustained tumor inhibition for 7 days following drug withdrawal (Fig. 4c, d). We tested two KRAS G12C-mutated colorectal cancer patient-derived xenograft models (PDX), one KRAS G12V and one KRAS Q61K mutant pancreatic PDX model and observed improved antitumor activity using a combination of BI-3406 with trametinib (Fig. 4e, f and Supplementary Fig. S4d–g). As expected based on proliferation assays using KRAS Q61 mutant cells, monotherapy of BI-3406 resulted in only weak efficacy in monotherapy in the KRAS Q61K mutant PDX model, yet the SOS1 and MEK inhibitor combination significantly improved antitumor activity as compared to both monotherapies (p=0.0026; Supplementary Fig. S4g). The combination treatment was very well tolerated (Supplementary Fig. S4b–c, S4h–k). As SOS2 may promote resistance to SOS1 over time, we analyzed the colorectal PDX model B8032, but found no compensatory upregulation of SOS2 mRNA levels upon 21 days of treatment with both SOS1 and MEK inhibitor (Supplementary Fig. S4l–m).

The SOS1 inhibitor BI-3406 prevents adaptive resistance to MEK inhibition

The mechanism underlying the SOS1/MEK inhibitor combination efficacy was evaluated with regards to the impact on modulation of the KRAS-RAF-MEK-ERK cascade. *In vitro* MEK inhibitor treatment at clinically relevant doses, in the low nM-range (see description in Supplementary Data), resulted in a progressive increase of MEK1/2 Ser217/221 phosphorylation, an effect termed adaptive resistance or negative feedback relief (Fig. 5a and Supplementary Fig. S5a) (17). Consistent with our hypothesis that a SOS1 inhibitor might counteract adaptive resistance to MEK inhibition, combination of BI-3406 and trametinib antagonized the MEK inhibitor-induced increase of MEK1/2 phosphorylation in MIA PaCa-2 cells (Fig. 5a, and Supplementary Data Fig. 5a and b). A moderate, yet statistically significant effect on pERK1/2 levels was detected after 24–72 hours of treatment with BI-3406, whereas a marked reduction of ERK1/2 phosphorylation was observed with trametinib (Fig. 5b, Supplementary Fig. S5c). An additional reduction in pERK levels was observed upon combination of both drugs (Fig. 5b and Supplementary Fig. S5c). This effect was also observed in NCI-H23 cells, a KRAS G12C mutant cell line, albeit to a lesser degree (Supplementary Fig. S5d). A combination of BI-3406 and trametinib resulted in a near-complete reduction of pERK1/2 phosphorylation compared to the partial effects induced by the two monotherapies in MIA PaCa-2 tumor bearing mice (Fig. 5c). Combination of the SOS1 inhibitor and MEK inhibitor elicited a reduction of pERK and blockade of adaptive resistance, measured by pMEK1/2 in MIA PaCa-2 and NCI-H23 cells, not only when grown in 2D (Fig5a–b and Supplementary Fig. 5a–d) but also when cultured in 3D (Supplementary Fig. S5e–h). Furthermore, we observed that the combination of MEK and SOS1 inhibition resulted in an enhanced reduction of pERK and S6 phosphorylation as assessed by Reverse Phase Protein Array (RPPA) analysis in two colorectal cancer patient-derived xenograft models (Supplementary Fig. S5i and Table S8). In addition, the combination led to enhanced reduction of DUSP6 mRNA in MIA PaCa2 tumors (Supplementary Fig. S5j) and augmented induction of apoptosis as shown in the KRAS-driven cell line DLD1 (Supplementary Fig. S5k).

Finally, we investigated whether the beneficial effect of BI-3406 described above could be extended to a direct KRAS inhibitor, the clinical KRAS G12C inhibitor AMG 510. Strikingly the combination of AMG 510 with BI-3406 resulted in stronger and more prolonged suppression of pERK, as compared to AMG 510 monotherapy in NCI-H358 (KRAS G12C) cells *in vitro* (Supplementary Fig. S5l). The addition of the SOS1 inhibitor to AMG 510 largely prevented the rebound of pERK at the 72h time point. A similar effect was observed at 72h upon combination of AMG 510 with the SHP2 inhibitor SHP099 (Supplementary Fig. S5l).

In summary, the SOS1 inhibitor BI-3406 enhances the extent and duration of MAPK pathway inhibition upon combination with a MEK or KRAS G12C inhibitor, suggesting it is able to counteract adaptive resistance. This highlights SOS1 inhibition as a promising combination option for MAPK pathway and direct KRAS inhibitors. In line with this, we show that a SOS1/MEK inhibitor combination enables long-term pathway inhibition resulting in tumor regressions in multiple KRAS-driven cancer models at well-tolerated doses (Fig. 5d).

Discussion

KRAS mutations are the most frequent gain-of-function alterations found in cancer patients, yet KRAS-driven tumors are largely refractory to anticancer therapies. Despite more than two and a half decades of research describing the central role of SOS1 in developmental and oncogenic signaling pathways, most notably in the direct activation of RAS oncoproteins (37–40), no SOS1 inhibitor has progressed to the clinic. The previously described catalytic SOS1 modulator BAY293 (28) inhibited cancer cell proliferation with weak potency and irrespective of *KRAS* status. Here we describe a highly potent and selective small molecule inhibitor, BI-3406, that binds to SOS1 and thereby blocks protein-protein interaction with RAS-GDP. BI-3406 is the first example of an orally bioavailable SOS1::KRAS interaction inhibitor that reduces RAS-GTP levels and curtails MAPK pathway signaling *in vitro* and *in vivo*. BI-3406 limits the growth of the majority of tumor cells driven by KRAS variants at positions G12 and G13, as shown in 3D proliferation assays. As tumors bearing these KRAS mutations are most prevalent in colorectal cancer, pancreatic cancer and non-small cell lung cancer, these results provide compelling evidence that the SOS1::KRAS interface is a druggable target of potential clinical importance, and highlight BI-3406 as a front-runner of a new generation of GDP-KRAS-directed inhibitors with promising therapeutic potential. In contrast to covalent KRAS G12C-specific inhibitors (12,14), this novel approach holds promise for impact across the majority of mutant KRAS alleles, including the two most prevalent variants G12D and G12V. Interestingly, our data suggest that tumors harboring codon 61 mutations (such as Q61H), appear to be less sensitive to SOS1 inhibition, possibly because these mutant isoforms have the lowest intrinsic GTPase activity and may require less upstream signaling to remain GTP bound (41). The KRAS G12R variant, which is relatively common in pancreatic cancers (~20% prevalence), showed no modulation of pERK following treatment with BI-3406. This finding is in line with a recent publication describing an inability of the catalytic domain of SOS1 to interact with this KRAS G12R mutant oncoprotein (31). The sensitivity spectrum we have observed towards SOS1 inhibition further supports the concept of oncogenic KRAS G12 and G13 variants functioning in a semi-autonomous manner (42) and remain susceptible to regulation by SOS1 for optimal GTP-loading. Collectively, our data suggest that BI-3406 will be able to impact about 80–90% of all KRAS-driven cancers.

We have carried out a comprehensive screen for effective combination partners. Synergy was observed upon combination of SOS1 with MEK inhibitors, leading to tumor regressions in multiple mutant KRAS-driven cancer models at well tolerated doses. Of the two SOS isoforms, SOS1 and SOS2, only SOS1 is phosphorylated by ERK, resulting in the reduction of its GEF activity (26). Treatment with a MEK inhibitor reduces the activity of ERK1/2, resulting in release of a negative feedback loop, thus increasing the activity of SOS1-mediated formation of GTP-loaded KRAS (25,26). Combination of MEKi with BI-3406 thus blocks the negative feedback release by reducing pMEK1/2 and pERK1/2 levels, supporting sustained pathway inhibition and tumor regressions (Fig. 5d). Tumor stasis was observed with a SOS1/MEK inhibitor combination in colorectal and pancreatic PDX models. This may indicate that, in these tumor types, additional feedback and bypass mechanisms are effective, and triple combinations are needed to shut down KRAS signaling

and achieve tumor regressions. Due to the favorable tolerability of the SOS1/MEK treatment, combinations with standard of care treatments will be further evaluated with the aim to achieve tumor regressions in colorectal and pancreatic cancer models. We demonstrated that, in addition to the combination of BI-3406 with trametinib (MEKi), combination of BI-3406 with the clinical KRAS G12C inhibitor AMG 510 (KRASG12Ci) results in enhanced and prolonged MAPK pathway suppression. Our study highlights SOS1 inhibitors as promising combination partners for inhibitors directly targeting KRAS, the GDP-bound form of KRAS, or downstream MAPK pathway intermediates. This finding is also in line with a recent report describing a marked synergy in NSCLC cell lines combining SOS1 inhibition with vertical EGFR inhibition (43).

BI-3406 is a selective inhibitor of SOS1 and does not target the paralog GEF SOS2. Simultaneous genetic inactivation of both SOS proteins leads to rapid death in mouse models, in contrast to single gene perturbations (44). Thus, while the SOS1 selectivity may reduce the monotherapy impact of BI-3406 on KRAS and the MAPK pathway, it can facilitate combination therapies due to the expected superior tolerability of a SOS1 specific inhibitor compared to a pan SOS1/SOS2 inhibitor (44,45). Furthermore, targeting SOS1 can selectively exploit its key function in adaptive feedback control that is not shared with its paralogue SOS2 (25,26). No upregulation of SOS2 expression was observed in our biomarker and efficacy experiments. It remains to be determined whether cancer patients treated with a SOS1 inhibitor will exhibit induction of SOS2 levels.

Recently, inhibitors targeting the protein-tyrosine phosphatase SHP2 (encoded by the gene *PTPN11*), a common node downstream of RTKs that is required for RAS activation, have been reported (18,19). Interestingly, these reports also suggest that inhibition of SHP2 can attenuate adaptive MEK inhibitor resistance in KRAS-dependent cancers (46–49). Our comparative analysis of the SHP2 inhibitor tool compound SHP099, suggest activity in cell lines harboring G12C, a subset of G12D and possibly G12S KRAS variant driven cell lines, while the SOS1 inhibitor BI-3406 demonstrates activity in all KRAS G12 and G13 mutant cell lines tested, with the exception of cell lines driven by the G12R oncoprotein. While only BI-3406 is active in the KRAS G13-driven context, both inhibitors lack single agent activity in KRAS Q61 mutant cell lines, suggesting an overall broader impact on KRAS mutant cancers by the SOS1 inhibitor. Future studies will be required to compare and contrast the capabilities of SOS1 and SHP2 inhibitors to overcome adaptive resistance to KRAS/RAF/MEK/ERK-targeted agents across KRAS-driven cancers.

While the precise mechanism by which SHP2 contributes to KRAS activation is yet to be determined, SHP2 is not a direct activator of KRAS and may in part act via SOS1 (50,51). Ongoing clinical evaluations will show if SOS1i/MEKi and SHP2i/MEKi combinations will differ in terms of safety and response rates across tumors with different KRAS alterations.

Collectively, our study provides a new chemical probe for further dissection of the cellular functions of SOS1 in tumorigenesis and MEK inhibitor-driven drug resistance. Importantly, the pharmacological properties of BI-3406 and close analogues hold the promise of developing clinical SOS1 compounds that, in combination with MEK inhibitors and potentially other RTK/MAPK pathway inhibitors, could provide significant clinical benefit

across a broad patient population currently lacking molecularly targeted, precision medicine options. A Phase 1 clinical trial has been initiated (NCT04111458) for patients with advanced *KRAS*-mutated cancers to evaluate safety, tolerability, pharmacokinetic and pharmacodynamic properties, and preliminary efficacy of BI 1701963, a SOS1::KRAS inhibitor closely related to BI-3406, alone and in combination with the MEK inhibitor trametinib.

Methods

Additional descriptions of methods can be found in the Supplementary Data file.

Cell culture—Tumor cell lines were obtained from the American Type Culture Collection (Manassas, US-VA) or the German Collection of Microorganisms and Cell Culture (DSMZ, Braunschweig, Germany). All cell lines used in this study were cultured according to the manufacturer's instruction and authenticated by short tandem repeat (STR) analysis at Boehringer Ingelheim (Supplementary Table S9). With regard to the 2D proliferation assays, cells were seeded in their respective medium supplemented with 2% FCS. For the 3D proliferation assay, the cells were embedded in soft agar, which required three separate layers within a well; a bottom layer formed of 1% agar solution, a cell layer formed of a 0.3% agar solution and a medium layer (described in detail in the supplemental data). BI-3406, trametinib or a positive control (e.g. panobinostat) was added with increasing concentrations. Readout of cell proliferation was adopted on cell growth properties avoiding more than 80% confluence in the control wells. Dependent on the individual doubling times, readout for individual cell lines was between 5 and 14 days. Number of living cells were quantified through the addition of AlamarBlue® reagent or CellTiter-Glo (Promega). As inhibition of the SOS1::KRAS inhibitor results in most cases in only 50% reduction of proliferation, the IC_{50} values describe the point of inflection of a curve and this does not fit in all cases with 50% inhibition. Transfection of cells, generation of isogeneic NCI-H23 cells, generation of SOS1 or SOS2 negative cells lines as well as the transgeneic expression of FLAG-SOS1 variants can be found in supplementary data and tables S10 and S11. Details on immunodetection in cell lysate can be found in supplementary data and tables S10, S11 and S12.

Synthesis of BI-3406—Conditions are described in the supplementary data section. A schematic representation of the synthesis can be found in Supplementary Fig. S1e and S1f.

Protein-protein interaction assays (AlphaScreen assay technology)—Details on protein expression and purification can be found in supplementary data. Measurements of various protein–protein interactions were performed using the Alpha Screen technology developed by Perkin Elmer. Recombinant KRAS proteins, based on KRAS isoform 4B (uniprot id P01116–2) were: KRAS G12D (1–169, N-terminal 6His-tag, C-terminal avi-tag) from Xtal BioStructures, Inc., KRAS G12C (1–169, C-terminal avi-tag, biotinylated, mutations: C51S, C80L, C118S). Biotinylation was performed *in vitro* with recombinant BirA biotin-protein ligase as recommended by the manufacturer (Avidity LLC, Aurora, Colorado, USA). Interacting proteins such as SOS1 (564–1049, N-terminal GST-tag, TEV cleavage site) and SOS2 (562–1047, N-terminal GST-tag, TEV cleavage site) were

expressed as glutathione S transferase (GST) fusions. Accordingly, the Alpha Screen beads were glutathione coated Alpha Lisa acceptor beads (Perkin Elmer AL 109 R) and Alpha Screen Streptavidin conjugated donor beads (Perkin Elmer 6760002L). Nucleotide was purchased from Sigma (GDP #G7127) and Tween-20 from Biorad (#161–0781). All interaction assays were carried out in PBS, containing 0.1% bovine serum albumin, 0,05% Tween-20 and 10 μM GDP. Assays were carried out in white ProxiPlate-384 Plus plates (Perkin Elmer #6008280) in a final volume of 20 μL. In brief, biotinylated KRAS proteins (10 nM final concentration) and GST-SOS1 or GST-SOS2 (10 nM final) were mixed with glutathione acceptor beads (5 μg/mL final concentration) in buffer, containing GDP and were incubated for 30 min at room temperature. After addition of streptavidin donor beads (5 μg/mL final concentration) under green light, the mixture was further incubated for 60 min in the dark at room temperature. Single oxygen induced fluorescence was measured at an Enspire multimode plate reader (Perkin Elmer) according to the manufacturer's recommendations. Data were analyzed using the GraphPad Prism based data software.

Measurement of KRAS-GTP levels—RAS-GTP levels were analyzed using a RAS G-LISA assay kit (Cytoskeleton Inc., Denver, CO, USA, #BK131) according to the manufacturer's instructions. Briefly, 600,000 cells were seeded in 6 wells and grown to 70% confluence. Cells were washed with ice-cold PBS and lysed in 80 μL ice-cold lysis buffer supplemented with the provided protease inhibitor cocktail. Lysates were quickly frozen in liquid nitrogen and stored at −80°C until further usage. After normalizing protein concentration, 40 μg of protein was added in duplicates to wells of the RAS G-LISA plate coated with RAS GTP-binding protein and incubated at 4°C for 30 minutes while shaking at 400 rpm. After washing, antigen presenting buffer was added for 2 minutes. To measure bound RAS GTP levels, wells were subsequently incubated with an anti-RAS primary antibody (1:50) followed by a HRP-labelled secondary antibody (1:500) and finally by adding a HRP detection reagent. Absorbance was measured by 490 nm using an EnSpire Multimode Reader (Perkin Elmer). Background was determined by a negative control well and subtracted from all samples. The same assay was used to determine amount of RAS-GTP levels in tumor lysate.

Biomarker and PK/PD analysis—pERK and pAKT modulation in tumors was determined using the Phospho/Total ERK1/2, Phospho(Ser473)/Total Akt and Phospho-Akt (Thr308) Whole Cell Lysate Kits (MesoScale, K15107D, K15100D and K151DYD). Tumors were homogenized using Ready Prep Mini Grinders (#163–2146 BIO RAD) and lysed in MSD TRIS Lysis Buffer plus inhibitors (as provided in the kit). Protein concentration was determined by Bradford analysis. 0.8 μg/μL were used for pERK measurements (biological replicates) according to the recommendations of the manufacturer. Signal intensities were measured using a MESO SECTOR S 600 reader. The pERK to total ERK ratio was calculated and the data plotted in Graphpad PRISM. This assay was used as well for measurement of PD modulation in several tumor cell lines (Supplementary Figure S2e).

pERK levels were determined in mouse skin based on IHC staining (H-scores). Immunohistochemistry (IHC) was performed on formalin-fixed, paraffin-embedded tissue, 3

μm sections using anti-Phospho-p44/42 MAPK (Erk1/2) (Thr202/Tyr204) (1:40, CST) Antibody incubation and detection were carried out at 37°C. Antigen retrieval was performed using Thermo PT module with buffer pH6 (Dako #K8005) and visualized using the EnVision kit (Dako, Glostrup, Denmark). Appropriate positive and negative controls were included with the study sections. Digital images of whole tissue sections were acquired using a Aperio AT2 histology scanner (Leica Microsystems). Images were evaluated by a pathologist (FT) and H-Score was generated using HALO software 3.0, Indica Lab©.

RNA isolation and sequencing library preparation for expression profiling— Cells were lysed in TRI lysis reagent (Qiagen, #79306) according to the manufacturer's instructions. Instead of chloroform, 10% volume 1-bromo-2-chloropropane (SigmaAldrich, #B9673) was added. Total RNA was isolated with RNAeasy Mini Kit (Qiagen, #73404). Quant-seq libraries were prepared using the QuantSeq 3' mRNA-Seq Library Prep Kit FWD for Illumina from Lexogene (#015.96) according to manufacturer's instructions. Samples were subsequently sequenced on an Illumina NextSeq 500 system with a single-end 76bp protocol. Single-end sequencing reads from grafted samples were filtered into human and mouse reads using Disambiguate (52) based on mapping to hg38 and mm10. The filtered reads were then processed with a pipeline building upon and extending the implementation of the ENCODE "Long RNA-seq" pipeline. Additional details on the methods are outlined in the Supplementary Information.

Whole-exome sequencing—In-house DNA libraries were prepared using the Agilent SureSelectXT Human AllExon 50 Mb enrichment kit and subsequently sequenced on an Illumina HiSeq 2000 with a 100 bp paired-end protocol. Sequencing data from in-house cell lines was completed with data retrieved from CCLE and COSMIC.

Analysis of gene expression by QuantiGene single plex technology (Affymetrix)—RNA was isolated from tumors as described above. The following probes were used: *DUSP6* (SA-11958) and *GAPDH* (SA-10001). The analysis was performed according to manufacturer's recommendations. The *DUSP6* levels of the individual tumors were normalized to their respective GAPDH levels.

Variant calling from whole-exome sequencing data (DNA-seq)—Paired-end sequencing reads were mapped against the human genome hg38 using bwa. We used strelka2 and the Ensembl Variant Effect Predictor for variant calling and annotation. In addition, data from COSMIC and CCLE was re-annotated and used to extend internal data. Additional details on the methods are outlined in the Supplementary Information. Additional details on the methods are outlined in the Supplementary Information.

Cell line derived efficacy studies and biomarker studies in mice—All animal studies were approved by the internal ethics committee and the local governmental committee. Group size in efficacy studies have been selected after performing power analysis. Female BomTac:NMRI-*Foxn1^{nu}* mice were used in all xenograft studies. For biomarker and efficacy experiments with MIA PaCa-2 female mice were engrafted subcutaneously with 10 million cells suspended in Matrigel. In case of biomarker studies with MIA PaCa-2 tumors, mice were randomized by tumor size in groups of 5 mice once

tumors reached a size of 170–500 mm³. Mice were treated once at time point 0 hour and 6 hours. Tumors were explanted and snap frozen to analyze biomarker modulation. Details of bioanalysis of mouse blood samples can be found in the supplementary data.

In case of efficacy experiments, mice were randomized in groups (n=7 mice per treatment group) by tumor size by the automated data storage system Sepia on day 7 (Fig. 3d) or 12 (Fig. 4.a) once tumors reached a size between 95–180 mm³. Compound treatment was initiated after randomization based on body weight. Tumor size was measured by an electronic caliper and body weight was monitored daily. The analysis follows largely the procedures described in (53,54). Number of subcutaneous cells injected and size for tumor randomization was as following with a group size of 7–10 mice: A549 (10 million cells; 62–150 mm³; n=7, Fig. 3f and Supplemental data Fig. 3g and 3h), LoVo (10 million cells; 123–173 mm³; n=7, Fig. 3f and 4f), SW620 (5 million cells, 80–125 mm³, Fig. 3f) and A375 (5 million cells, 64–149 mm³, n=6–7, Fig. 3f). In case of the biomarker studies with A549 cells, mice were randomized once tumors reached a size between 209 and 320 mm³ (Supplemental data Fig. 3b and c)). BI-3406 was dissolved in 0.5% Natrosol. Trametinib was dissolved in 0.5% DMSO and 0.5% Natrosol. The control group was treated with 0.5% of Natrosol orally in the same frequency as in the treatment groups (twice daily). All compounds were administered intragastrically by gavage (10 mL/kg). Details on formulation of compounds can be found in supplementary data.

Patient derived xenograft studies—PDX model characterization and profiling is described in detail in the supplementary data and Table S13. PDX tumor fragments (4×4×4 mm3) were implanted on the right hind flanks of NSG female mice purchased from Jackson Laboratory and allowed to grow to an average volume of 100–250 mm3 as monitored by calliper measurements. At enrolment, animals were randomized and treated orally on a 5 days on/2 days off schedule for convenience, to avoid weekend treatments, with Vehicle (0.5% Natrosol), bid (6 hours apart), BI-3406 (SOS1i) at 50 mg/kg, bid (6 hours apart), trametinib at 0.1 mg/kg, bid (6 hours apart), or the combination thereof. Mice were 11 weeks old and treatment group sizes included at least 5–7 mice per group. All animals received LabDiet 5053 chow ad libitum. trametinib was purchased from ChemieTek. In the patient derived xenograft studies tumor growth was monitored two times a week with calipers and the tumor volume (TV) was calculated as $TV = (D \times d2/2)$, where "D" is the largest and "d" is the smallest superficial visible diameter of the tumor mass. All measure are documented as mm³. Body weights were measured twice weekly and used to adjust dosing volume and monitor animal health. RPPA analysis of explanted tumor material is described in detail in the supplementary data section (Supplementary Figure S5i and Table S8).

Statistical analysis—Statistical analyses and Bioinformatics analysis were performed with R version 3.5.0 & Bioconductor 3.7 or GraphPad Prism. A Fisher's exact test was used for computing the associations of gene mutations with the sensitivity status of cell lines and for comparison of tumor volumes from the control the group with one treatment group. For calculations of tumor volume, absolute values were used for statistical analysis. Due to the observed variation, nonparametric methods were applied. In case several treatment groups were compared one-sided non-parametric Mann-Whitney-Wilcoxon U-tests were applied to

compare treatment groups with the control, as reduced tumor growth was expected following treatment. The p values for the tumor volume (efficacy parameter) were adjusted for multiple comparisons according to Bonferroni-Holm within each subtopic (comparisons versus control, comparisons mono therapies versus combination therapy) whereas the p values of the body weight (tolerability parameter) remained unadjusted in order not to overlook a possible adverse effect. The level of significance was fixed at $\alpha = 5\%$. An (adjusted) p value of less than 0.05 was considered to show a statistically significant difference between the groups and differences were seen as indicative whenever 0.05 p-value < 0.10. Data are represented as dot plots with bar graphs for mean ± standard deviation (s.d.) or standard error of the mean (s.e.m.), as indicated. In case of the PDX experiments statistical significance was determined using an unpaired t-test per row and the Holm-Sidak method to correct for multiple comparisons (Fig. 4e and f and Supplementary Fig. S4d–f)

Data availability—Atomic coordinates and structure factors for the co-crystal x-ray structures of BI-68BS and BI-3406 and SOS1 have been deposited at the Protein Data Band under accession number 6SFR (BI-68BS) and 6SCM (BI-3406). Data is available in Supplementary Table S1. Expression data generated and analyzed in this study have been deposited in the Gene Expression Omnibus (GEO) database under the accession numbers GSE128385. Processed data is available in Supplementary Table S7.

Supplementary Material

Refer to Web version on PubMed Central for supplementary material.

Acknowledgements

References

1. Moll HP, Pranz K, Musteanu M, Grabner B, Hruschka N, Mohrherr J, et al. Afatinib restrains K-RAS-driven lung tumorigenesis. Science translational medicine 2018;10(446) doi 10.1126/scitranslmed.aao2301.

2. Cichowski K, Jacks T. NF1 tumor suppressor gene function: narrowing the GAP. Cell 2001;104(4):593–604 doi 10.1016/s0092-8674(01)00245-8. [PubMed: 11239415]

3. Bollag G, Clapp DW, Shih S, Adler F, Zhang YY, Thompson P, et al. Loss of NF1 results in activation of the Ras signaling pathway and leads to aberrant growth in haematopoietic cells. Nature genetics 1996;12(2):144–8 doi 10.1038/ng0296-144. [PubMed: 8563751]

4. Cox AD, Fesik SW, Kimmelman AC, Luo J, Der CJ. Drugging the undruggable RAS: Mission possible? Nature reviews Drug discovery 2014;13(11):828–51 doi 10.1038/nrd4389. [PubMed: 25323927]

5. Stephen AG, Esposito D, Bagni RK, McCormick F. Dragging ras back in the ring. Cancer cell 2014;25(3):272–81 doi 10.1016/j.ccr.2014.02.017. [PubMed: 24651010]

6. Cerami E, Gao J, Dogrusoz U, Gross BE, Sumer SO, Aksoy BA, et al. The cBio Cancer Genomics Portal: An Open Platform for Exploring Multidimensional Cancer Genomics Data. Cancer discovery 2012;2(5):401–4 doi 10.1158/2159-8290.Cd-12-0095. [PubMed: 22588877]

7. AACR Project GENIE: Powering Precision Medicine through an International Consortium. Cancer discovery 2017;7(8):818–31 doi 10.1158/2159-8290.Cd-17-0151. [PubMed: 28572459]

8. Chin L, Tam A, Pomerantz J, Wong M, Holash J, Bardeesy N, et al. Essential role for oncogenic Ras in tumour maintenance. Nature 1999;400(6743):468–72 doi 10.1038/22788. [PubMed: 10440378]

9. Fisher GH, Wellen SL, Klimstra D, Lenczowski JM, Tichelaar JW, Lizak MJ, et al. Induction and apoptotic regression of lung adenocarcinomas by regulation of a K-Ras transgene in the presence and absence of tumor suppressor genes. Genes & development 2001;15(24):3249–62 doi 10.1101/gad.947701. [PubMed: 11751631]

10. Ying H, Kimmelman AC, Lyssiotis CA, Hua S, Chu GC, Fletcher-Sananikone E, et al. Oncogenic Kras maintains pancreatic tumors through regulation of anabolic glucose metabolism. Cell 2012;149(3):656–70 doi 10.1016/j.cell.2012.01.058. [PubMed: 22541435]

11. Collins MA, Bednar F, Zhang Y, Brisset JC, Galban S, Galban CJ, et al. Oncogenic Kras is required for both the initiation and maintenance of pancreatic cancer in mice. The Journal of clinical investigation 2012;122(2):639–53 doi 10.1172/jci59227. [PubMed: 22232209]

12. Hallin J, Engstrom LD, Hargis L, Calinisan A, Aranda R, Briere DM, et al. The KRAS(G12C) Inhibitor MRTX849 Provides Insight toward Therapeutic Susceptibility of KRAS-Mutant Cancers in Mouse Models and Patients. Cancer discovery 2020;10(1):54–71 doi 10.1158/2159-8290.CD-19-1167. [PubMed: 31658955]

13. Canon J, Rex K, Saiki AY, Mohr C, Cooke K, Bagal D, et al. The clinical KRAS(G12C) inhibitor AMG 510 drives anti-tumour immunity. Nature 2019;575(7781):217–23 doi 10.1038/s41586-019-1694-1. [PubMed: 31666701]

14. Mullard A Cracking KRAS. Nature reviews Drug discovery 2019;18(12):887–91 doi 10.1038/d41573-019-00195-5.

15. Fakih M, O'Neil B, Price TJ, Falchook GS, Desai J, Kuo J, et al. Phase 1 study evaluating the safety, tolerability, pharmacokinetics (PK), and efficacy of AMG 510, a novel small molecule KRASG12C inhibitor, in advanced solid tumors. Journal of Clinical Oncology 2019;37(15_suppl):3003- doi 10.1200/JCO.2019.37.15_suppl.3003.

16. Kessler D, Gmachl M, Mantoulidis A, Martin LJ, Zoephel A, Mayer M, et al. Drugging an undruggable pocket on KRAS. Proceedings of the National Academy of Sciences of the United States of America 2019;116(32):15823–9 doi 10.1073/pnas.1904529116. [PubMed: 31332011]

17. Lake D, Correa SA, Muller J. Negative feedback regulation of the ERK1/2 MAPK pathway. Cellular and molecular life sciences : CMLS 2016;73(23):4397–413 doi 10.1007/s00018-016-2297-8. [PubMed: 27342992]

18. Chen YN, LaMarche MJ, Chan HM, Fekkes P, Garcia-Fortanet J, Acker MG, et al. Allosteric inhibition of SHP2 phosphatase inhibits cancers driven by receptor tyrosine kinases. Nature 2016;535(7610):148–52 doi 10.1038/nature18621. [PubMed: 27362227]

19. Nichols RJ, Haderk F, Stahlhut C, Schulze CJ, Hemmati G, Wildes D, et al. RAS nucleotide cycling underlies the SHP2 phosphatase dependence of mutant BRAF-, NF1- and RAS-driven cancers. Nature cell biology 2018;20(9):1064–73 doi 10.1038/s41556-018-0169-1. [PubMed: 30104724]

20. Ou SI, Koczywas M, Ulahannan S, Janne P, Pacheco J, Burris H, et al. A12 The SHP2 Inhibitor RMC-4630 in Patients with KRAS-Mutant Non-Small Cell Lung Cancer: Preliminary Evaluation of a First-in-Man Phase 1 Clinical Trial. Journal of Thoracic Oncology 2020;15(2):S15–S6 doi 10.1016/j.jtho.2019.12.041.

21. Mullard A Phosphatases start shedding their stigma of undruggability. Nature reviews Drug discovery 2018;17(12):847–9 doi 10.1038/nrd.2018.201.

22. Alessi DR, Cuenda A, Cohen P, Dudley DT, Saltiel AR. PD 098059 is a specific inhibitor of the activation of mitogen-activated protein kinase kinase in vitro and in vivo. The Journal of biological chemistry 1995;270(46):27489–94 doi 10.1074/jbc.270.46.27489. [PubMed: 7499206]

23. Freedman TS, Sondermann H, Friedland GD, Kortemme T, Bar-Sagi D, Marqusee S, et al. A Ras-induced conformational switch in the Ras activator Son of sevenless. Proceedings of the National Academy of Sciences of the United States of America 2006;103(45):16692–7 doi 10.1073/pnas.0608127103. [PubMed: 17075039]

24. Jeng HH, Taylor LJ, Bar-Sagi D. Sos-mediated cross-activation of wild-type Ras by oncogenic Ras is essential for tumorigenesis. Nature communications 2012;3:1168 doi 10.1038/ncomms2173.

25. Rozakis-Adcock M, van der Geer P, Mbamalu G, Pawson T. MAP kinase phosphorylation of mSos1 promotes dissociation of mSos1-Shc and mSos1-EGF receptor complexes. Oncogene 1995;11(7):1417–26. [PubMed: 7478566]

26. Corbalan-Garcia S, Yang SS, Degenhardt KR, Bar-Sagi D. Identification of the mitogen-activated protein kinase phosphorylation sites on human Sos1 that regulate interaction with Grb2. Molecular and cellular biology 1996;16(10):5674–82 doi 10.1128/mcb.16.10.5674. [PubMed: 8816480]

27. Burns MC, Sun Q, Daniels RN, Camper D, Kennedy JP, Phan J, et al. Approach for targeting Ras with small molecules that activate SOS-mediated nucleotide exchange. Proceedings of the National Academy of Sciences of the United States of America 2014;111(9):3401–6 doi 10.1073/pnas.1315798111. [PubMed: 24550516]

28. Hillig RC, Sautier B, Schroeder J, Moosmayer D, Hilpmann A, Stegmann CM, et al. Discovery of potent SOS1 inhibitors that block RAS activation via disruption of the RAS-SOS1 interaction. Proceedings of the National Academy of Sciences of the United States of America 2019;116(7):2551–60 doi 10.1073/pnas.1812963116. [PubMed: 30683722]

29. Singh A, Greninger P, Rhodes D, Koopman L, Violette S, Bardeesy N, et al. A gene expression signature associated with "K-Ras addiction" reveals regulators of EMT and tumor cell survival. Cancer cell 2009;15(6):489–500 doi 10.1016/j.ccr.2009.03.022. [PubMed: 19477428]

30. Zhou ZW, Ambrogio C, Bera AK, Li Q, Li XX, Li L, et al. KRASQ61H preferentially signals through MAPK in a RAF dimer-dependent manner in non-small cell lung cancer. Cancer research 2020 doi 10.1158/0008-5472.CAN-20-0448.

31. Hobbs GA, Baker NM, Miermont AM, Thurman RD, Pierobon M, Tran TH, et al. Atypical KRAS(G12R) Mutant Is Impaired in PI3K Signaling and Macropinocytosis in Pancreatic Cancer. Cancer discovery 2020;10(1):104–23 doi 10.1158/2159-8290.CD-19-1006. [PubMed: 31649109]

32. Krauthammer M, Kong Y, Bacchiocchi A, Evans P, Pornputtapong N, Wu C, et al. Exome sequencing identifies recurrent mutations in NF1 and RASopathy genes in sun-exposed melanomas. Nature genetics 2015;47(9):996–1002 doi 10.1038/ng.3361. [PubMed: 26214590]

33. Nissan MH, Pratilas CA, Jones AM, Ramirez R, Won H, Liu C, et al. Loss of NF1 in cutaneous melanoma is associated with RAS activation and MEK dependence. Cancer research 2014;74(8):2340–50 doi 10.1158/0008-5472.Can-13-2625. [PubMed: 24576830]

34. Loboda A, Nebozhyn M, Klinghoffer R, Frazier J, Chastain M, Arthur W, et al. A gene expression signature of RAS pathway dependence predicts response to PI3K and RAS pathway inhibitors and expands the population of RAS pathway activated tumors. BMC medical genomics 2010;3:26 doi 10.1186/1755-8794-3-26. [PubMed: 20591134]

35. Wagle MC, Kirouac D, Klijn C, Liu B, Mahajan S, Junttila M, et al. A transcriptional MAPK Pathway Activity Score (MPAS) is a clinically relevant biomarker in multiple cancer types. NPJ precision oncology 2018;2(1):7 doi 10.1038/s41698-018-0051-4. [PubMed: 29872725]

36. Gilmartin AG, Bleam MR, Groy A, Moss KG, Minthorn EA, Kulkarni SG, et al. GSK1120212 (JTP-74057) is an inhibitor of MEK activity and activation with favorable pharmacokinetic properties for sustained in vivo pathway inhibition. Clinical cancer research : an official journal of

the American Association for Cancer Research 2011;17(5):989–1000 doi 10.1158/1078-0432.Ccr-10-2200. [PubMed: 21245089]

37. Rogge RD, Karlovich CA, Banerjee U. Genetic dissection of a neurodevelopmental pathway: Son of sevenless functions downstream of the sevenless and EGF receptor tyrosine kinases. Cell 1991;64(1):39–48 doi 10.1016/0092-8674(91)90207-f. [PubMed: 1846090]

38. Bonfini L, Karlovich CA, Dasgupta C, Banerjee U. The Son of sevenless gene product: a putative activator of Ras. Science (New York, NY) 1992;255(5044):603–6 doi 10.1126/science.1736363.

39. Chardin P, Camonis JH, Gale NW, van Aelst L, Schlessinger J, Wigler MH, et al. Human Sos1: a guanine nucleotide exchange factor for Ras that binds to GRB2. Science (New York, NY) 1993;260(5112):1338–43 doi 10.1126/science.8493579.

40. Egan SE, Giddings BW, Brooks MW, Buday L, Sizeland AM, Weinberg RA. Association of Sos Ras exchange protein with Grb2 is implicated in tyrosine kinase signal transduction and transformation. Nature 1993;363(6424):45–51 doi 10.1038/363045a0. [PubMed: 8479536]

41. Hunter JC, Manandhar A, Carrasco MA, Gurbani D, Gondi S, Westover KD. Biochemical and Structural Analysis of Common Cancer-Associated KRAS Mutations. Molecular cancer research : MCR 2015;13(9):1325–35 doi 10.1158/1541-7786.Mcr-15-0203. [PubMed: 26037647]

42. Bivona TG. Dampening oncogenic RAS signaling. Science (New York, NY) 2019;363(6433):1280–1 doi 10.1126/science.aav6703.

43. Theard PLS E; Sealover NE; Linke AJ; Pratico DJ; and Kortum RL Marked Synergy by Vertical Inhibition of EGFR signaling in NSCLC: SOS1 as a therapeutic target in EGFR-mutated cancer. . eLife 2020;accepted.

44. Baltanas FC, Perez-Andres M, Ginel-Picardo A, Diaz D, Jimeno D, Liceras-Boillos P, et al. Functional redundancy of Sos1 and Sos2 for lymphopoiesis and organismal homeostasis and survival. Molecular and cellular biology 2013;33(22):4562–78 doi 10.1128/MCB.01026-13. [PubMed: 24043312]

45. Esteban LM, Fernandez-Medarde A, Lopez E, Yienger K, Guerrero C, Ward JM, et al. Ras-guanine nucleotide exchange factor sos2 is dispensable for mouse growth and development. Molecular and cellular biology 2000;20(17):6410–3 doi 10.1128/mcb.20.17.6410-6413.2000. [PubMed: 10938118]

46. Ruess DA, Heynen GJ, Ciecielski KJ, Ai J, Berninger A, Kabacaoglu D, et al. Mutant KRAS-driven cancers depend on PTPN11/SHP2 phosphatase. Nature medicine 2018;24(7):954–60 doi 10.1038/s41591-018-0024-8.

47. Mainardi S, Mulero-Sanchez A, Prahallad A, Germano G, Bosma A, Krimpenfort P, et al. SHP2 is required for growth of KRAS-mutant non-small-cell lung cancer in vivo. Nature medicine 2018;24(7):961–7 doi 10.1038/s41591-018-0023-9.

48. Wong GS, Zhou J, Liu JB, Wu Z, Xu X, Li T, et al. Targeting wild-type KRAS-amplified gastroesophageal cancer through combined MEK and SHP2 inhibition. Nature medicine 2018;24(7):968–77 doi 10.1038/s41591-018-0022-x.

49. Fedele C, Ran H, Diskin B, Wei W, Jen J, Geer MJ, et al. SHP2 Inhibition Prevents Adaptive Resistance to MEK Inhibitors in Multiple Cancer Models. Cancer discovery 2018;8(10):1237–49 doi 10.1158/2159-8290.Cd-18-0444. [PubMed: 30045908]

50. Torres-Ayuso P, Brognard J. Shipping Out MEK Inhibitor Resistance with SHP2 Inhibitors. Cancer discovery 2018;8(10):1210–2 doi 10.1158/2159-8290.Cd-18-0915. [PubMed: 30279193]

51. Mai TT, Lito P. A treatment strategy for KRAS-driven tumors. Nature medicine 2018;24(7):902–4 doi 10.1038/s41591-018-0111-x.

52. Ahdesmaki MJ, Gray SR, Johnson JH, Lai Z. Disambiguate: An open-source application for disambiguating two species in next generation sequencing data from grafted samples. F1000Research 2016;5:2741 doi 10.12688/f1000research.10082.2. [PubMed: 27990269]

53. Waizenegger IC, Baum A, Steurer S, Stadtmuller H, Bader G, Schaaf O, et al. A Novel RAF Kinase Inhibitor with DFG-Out-Binding Mode: High Efficacy in BRAF-Mutant Tumor Xenograft Models in the Absence of Normal Tissue Hyperproliferation. Molecular cancer therapeutics 2016;15(3):354–65 doi 10.1158/1535-7163.Mct-15-0617. [PubMed: 26916115]

54. Sanderson MP, Hofmann MH, Garin-Chesa P, Schweifer N, Wernitznig A, Fischer S, et al. The IGF1R/INSR Inhibitor BI 885578 Selectively Inhibits Growth of IGF2-Overexpressing Colorectal

Cancer Tumors and Potentiates the Efficacy of Anti-VEGF Therapy. Molecular cancer therapeutics 2017;16(10):2223–33 doi 10.1158/1535-7163.Mct-17-0336. [PubMed: 28729397]

Significance

To date, there are no effective targeted pan-KRAS therapies. In-depth characterization of BI-3406 activity and identification of MEK inhibitors as effective combination partners provide an attractive therapeutic concept for the majority of KRAS mutant cancers, including those fueled by the most prevalent mutant KRAS oncoproteins G12D, G12V, G12C and G13D.
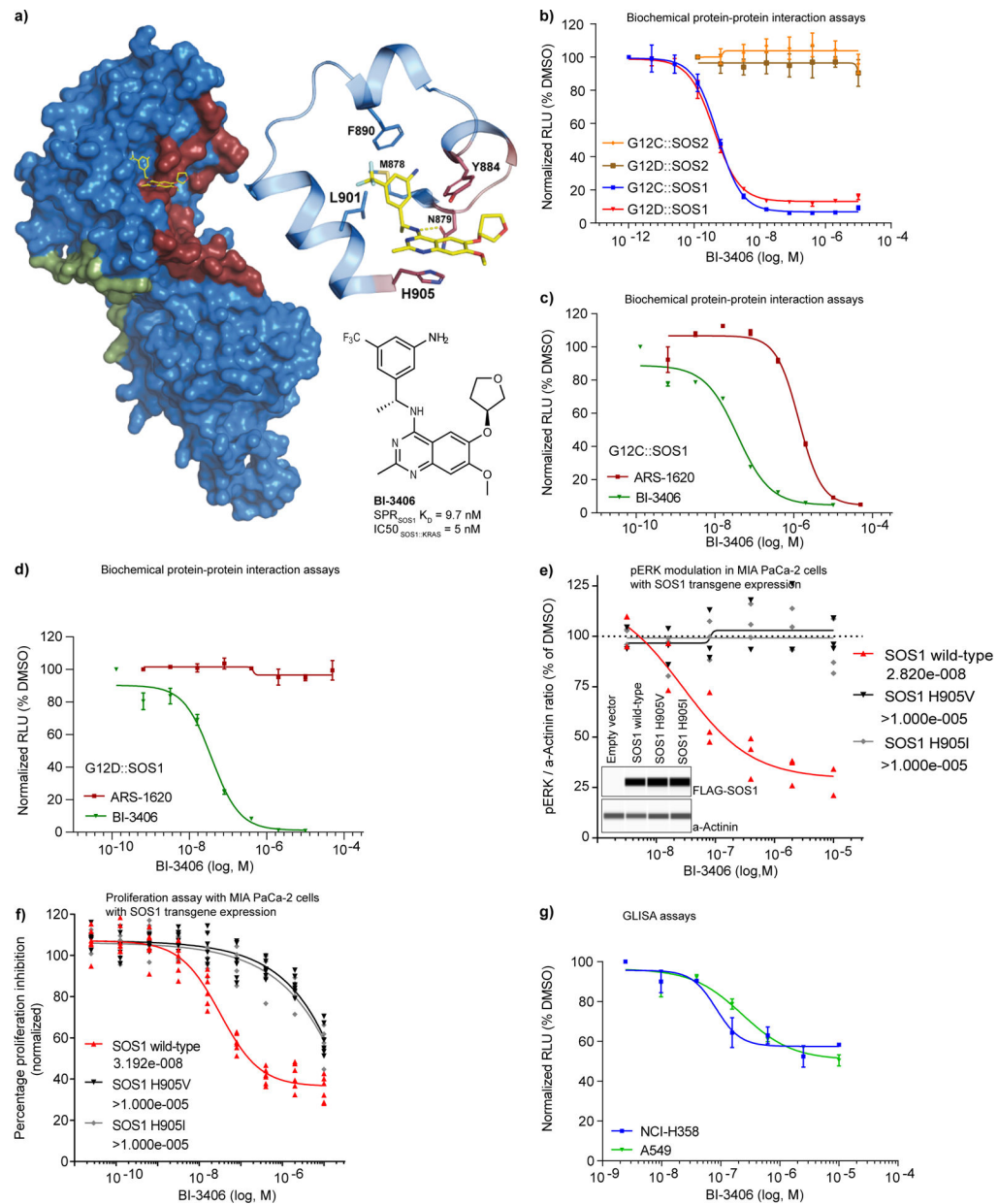
Figure 1: Discovery of BI-3406, a potent and selective SOS1::KRAS interaction inhibitor

a, Co-crystal x-ray structure of BI-3406 bound to the catalytic pocket of SOS1 (ligand shown in yellow, SOS1 as surface representation). The previously described catalytic RAS interaction site (dark red; PDB: 1NVU) and the allosteric site (green) are highlighted. The enlarged area depicts the key interactions of BI-3406 and SOS1 within the binding site. Amino acids involved in the RAS_{cat} interaction are highlighted in dark red, indicating a clash of BI-3406 with RAS_{cat}. Structure and potency of BI-3406 are shown at the bottom right. b, Biochemical protein-protein interaction assays (AlphaScreen) between recombinant SOS1 or SOS2 and recombinant KRAS G12C or KRAS G12D conducted under incubation with increasing concentrations of BI-3406 (dose-response curves as relative fluorescence units (RFUs) means±s.e.m., n=2). c-d, Biochemical protein-protein interaction assays

(AlphaScreen) between recombinant SOS1 and recombinant KRAS G12C (c) or KRAS G12D (d) carried out under increasing concentrations of BI-3406 or the covalent KRAS G12C inhibitor ARS-1620 (c, and d, n=2, means±s.e.m.). Dose response curves as in (b). e, MIA PaCa-2 stably transduced with FLAG-tagged wild-type SOS1 or the indicated mutant SOS1 transgenes were exposed to different concentrations of BI-3406 for 2 hours. Phospho-ERK levels were subsequently quantified in cell lysates by capillary immunodetection using alpha-actinin as a loading control and normalized to the levels measured in DMSO solvent treated samples (n=3 independent biological replicates). IC50 values (nM) are shown in the legend. Inlay: Lane view of FLAG-SOS1 transgene expression in comparison to alpha-actinin in stably transduced MIA PaCa-2 cells from a representative capillary immunodetection experiment. f, Cell proliferation assay using MIA PaCa-2 transgenic cell pools expressing the indicated FLAG-SOS1 transgenes (data points are derived from two independent biological replicates each containing three technical replicates). IC50 values (nM) are shown in the legend. g, Dose-dependent, cellular effect of BI-3406 on RAS-GTP levels (n=2, means±s.e.m.) in standard 2D / 10% serum conditions with increasing concentrations of BI-3406 for 2 h. RAS-GTP levels were quantified relative to DMSO controls (RAS G-LISA).
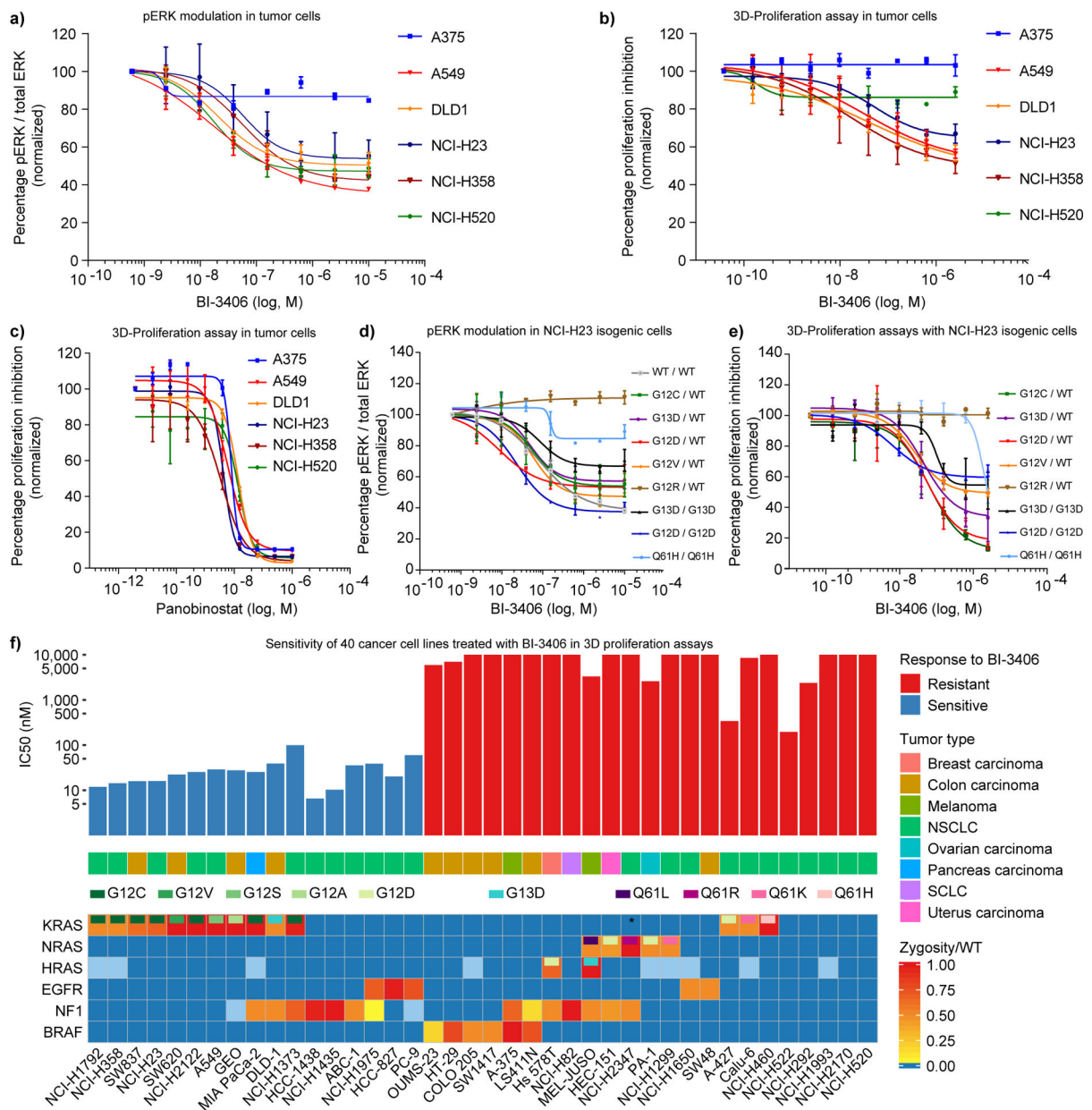
Figure 2: Drug sensitivity profiling of cancer cell lines uncovers an association of KRAS mutation status with sensitivity to SOS1 inhibition

a, Inhibition of pERK activity by BI-3406 after 1 hour in 2D assay conditions in a cancer cell line panel quantified by Western blotting (n=2, means±s.d.). A375 (KRAS wt, BRAF V600E), A549 (KRAS G12S), DLD-1 (KRAS G13D), NCI-H23 (KRAS G12C), NCI-H358 (KRAS G12C), and NCI-H520 (KRAS wt and BRAF wt). b, Inhibition of cell proliferation by BI-3406 in a cancer cell line panel in 3D proliferation assays (n=3, means±s.d.). c, *In vitro* sensitivity of a panel of cell lines to the positive control panobinostat (Sigma Aldrich) in a 3D proliferation assay (n=3, means±s.d.). d) Effect of BI-3406 on pERK levels in a panel of isogenic NCI-H23 cell lines. Values were normalized to total ERK protein (n=2, means±s.d.). e) *In vitro* sensitivity of a panel of isogenic cell lines treated with BI-3406 in a 3D proliferation assay (n=3, means±s.d.). f, *In vitro* sensitivity of 40 cancer cell lines treated

with BI-3406 in 3D proliferation assays. Panels depict the proliferation data (n=2), the respective cancer type, and the mutation status of selected genes. Cell lines are grouped based on an IC_{50} cut-off of 100 nmol/L. The mutation status and zygosity is shown by a continuous color-coding scheme, blue boxes reflect wild-type status, while light blue boxes indicate an unknown status. Only re-occurring hotspot mutations are reported for KRAS, NRAS, HRAS, EGFR, and BRAF (Supplementary Table S5). NCI-H2347 carries a KRAS L19F mutation (asterisks).
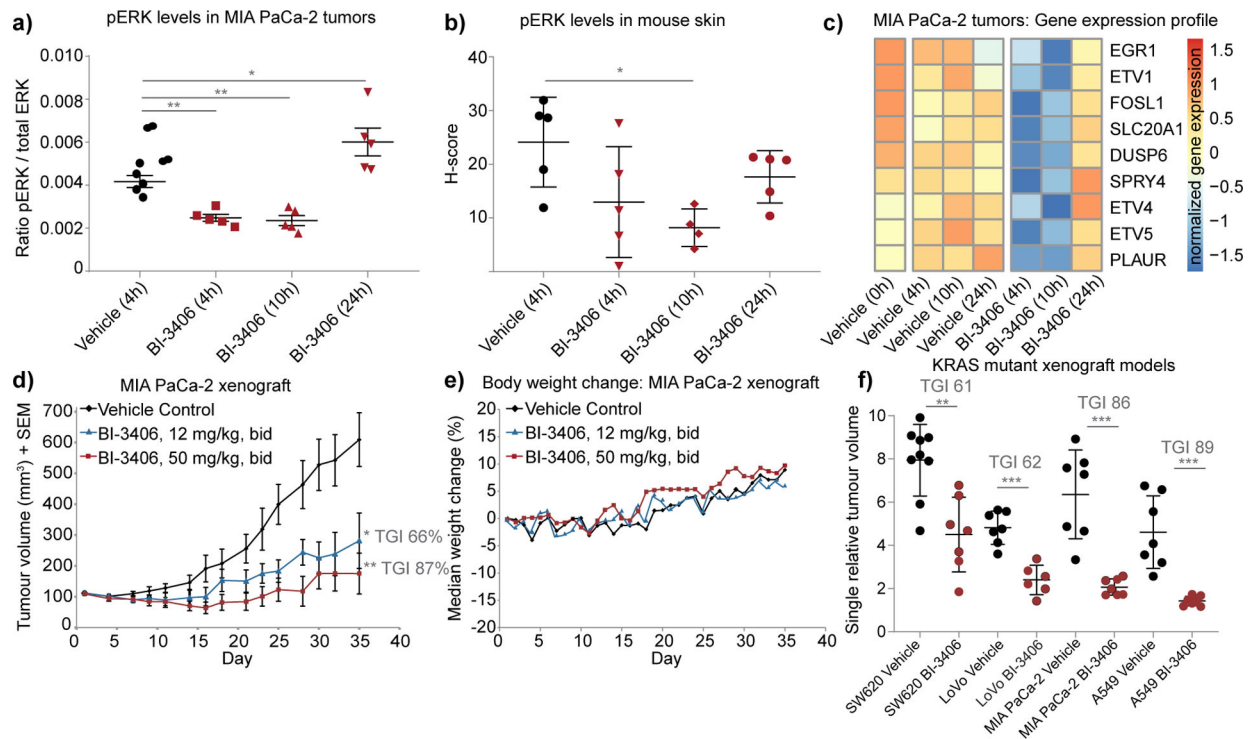
Figure 3: SOS1 inhibition suppresses tumor growth and KRAS/MAPK signaling in xenograft models of KRAS-driven cancers

a, pERK levels analyzed by a multiplexed immunoassay in explanted MIA PaCa-2 tumors treated with 50 mg/kg BI-3406 twice daily at the time point 0 h and 6 h. (n=5 animals per group, means±s.e.m, two-tailed t-test). b, pERK levels in mouse skin (treatment as in a) assessed by IHC staining (H-scores) (n=5 animals per group, means±s.d., two-tailed t-test). c, Gene expression profiling of pharmacodynamic biomarkers in a MIA PaCa-2 *in vivo* biomarker experiment (n=4–5 animals per group, medians of normalized gene expression). A subset of nine genes shows time-dependent modulation after BI-3406 (50 mg/kg) treatment, visualized as a color-coded expression heatmap. d, Anti-tumor effect of BI-3406 in the MIA PaCa-2 xenograft model (n=7 animals per group, means±s.e.m., one-tailed t-test) e, Median body weight change of mice bearing subcutaneous MIA PaCa-2 xenografts administered as described in (d) (n=7 animals per group, medians). f, Responses of different xenograft models after treatment with BI-3406 (50 mg/kg *bid*) or vehicle (control). Tumor growth inhibition (TGI) was determined based on tumor size after 20–23 days of continuous treatment (n=7–9 animals per group, means±s.d.). Genotypes of tested xenograft models: SW620 colorectal (KRAS G12V, BRAF wt), LoVo colorectal (KRAS G13D, BRAF wt), MIA PaCa-2 pancreas (KRAS G12C, BRAF wt), and A549 non-small cell lung cancer (KRAS G12S, BRAF wt). Significant TGI was achieved in all tested KRAS mutant xenograft models, with the exception of the KRAS wild-type model A375 (* 0.05 ** < 0.01, *** < 0.001, one tailed t-test).
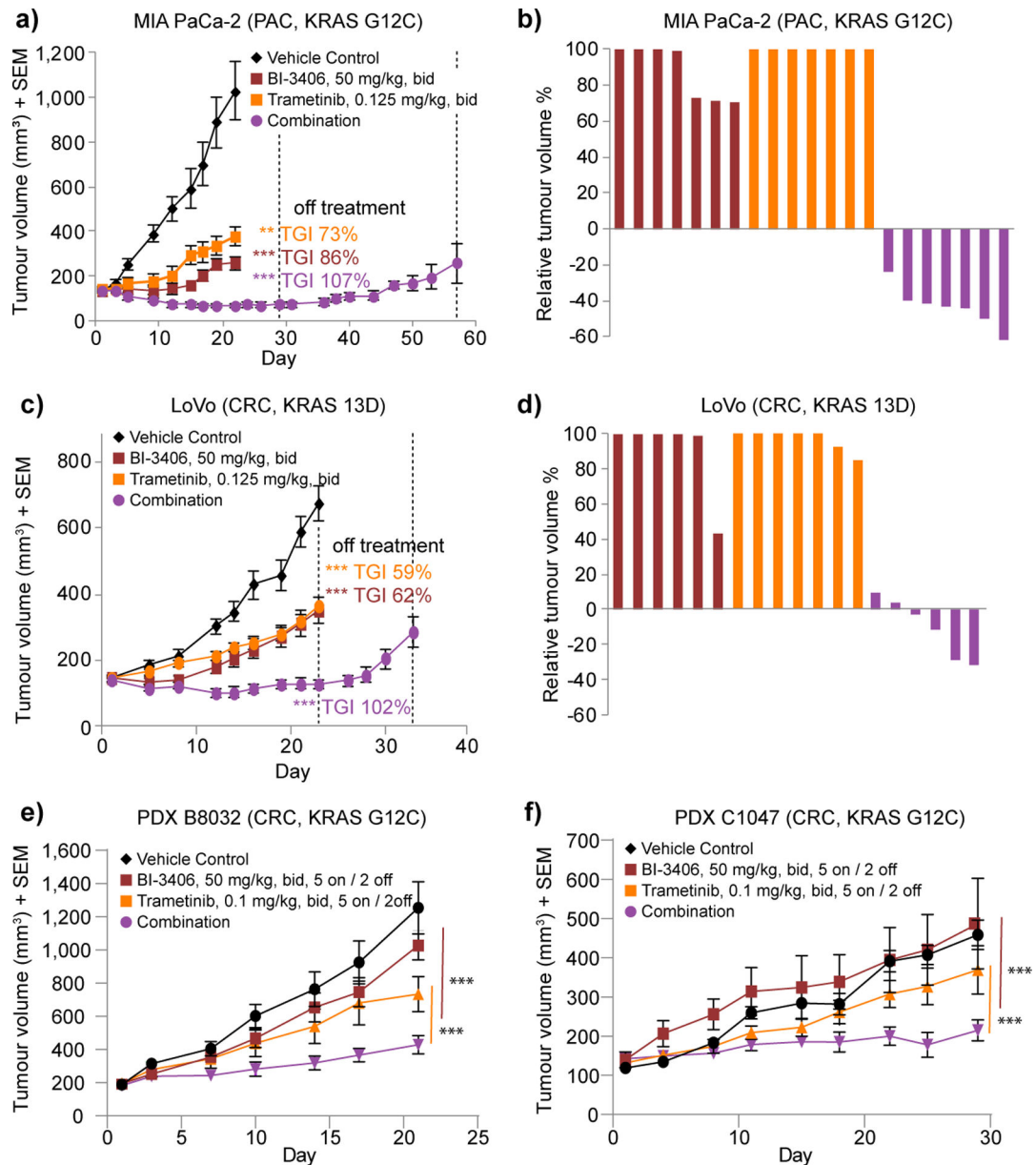
Figure 4: Combined SOS1 and MEK inhibition leads to regressions in KRAS-mutant tumors
a, Tumor volumes of mice injected subcutaneously with MIA PaCa-2 cells. All mice were
treated bid (with a delta of 6 hours) with vehicle (control), trametinib (0.125 mg/kg),
BI-3406 (50 mg/kg) for 22 days, or the combination of both agents for 29 days (n=7 animals
per group, means±s.e.m.) followed by an off-treatment period until day 57. b, Relative tumor
volume of MIA PaCa-2 are indicated as percent change from baseline at day 22. Values
smaller than zero percent indicate tumor regressions. c, Efficacy of the combination of
BI-3406 and trametinib in the LoVo xenograft model. Continuous treatment with trametinib
or BI-3406 alone or in combination for 23 days, followed by an off-treatment period until
day 34 (n=7 animals per group, means±s.e.m.). (* 0.05 ** < 0.01, *** < 0.001; a and c, one
tailed Student's t-test comparing control with treatment groups). d, Relative tumor volume

for the LoVo model are indicated as percent change from baseline at day 22. e-f Tumor growth of colorectal cancer (CRC) PDX xenografts in mice treated with vehicle, BI-3406 (50 mg/kg, *bid*), trametinib (0.1 mg/kg, *bid*), or the combination for the models B8032 (e) and C1047 (f) tumors (n=5–7 animals per group, means±s.e.m. For convenience in PDX models mice were treated in a 5 days on / 2 days off schedule. Statistical significance was determined using an unpaired t-test per row and the Holm-Sidak method to correct for multiple comparisons, see as well Supplementary Fig. S4d and S4e).
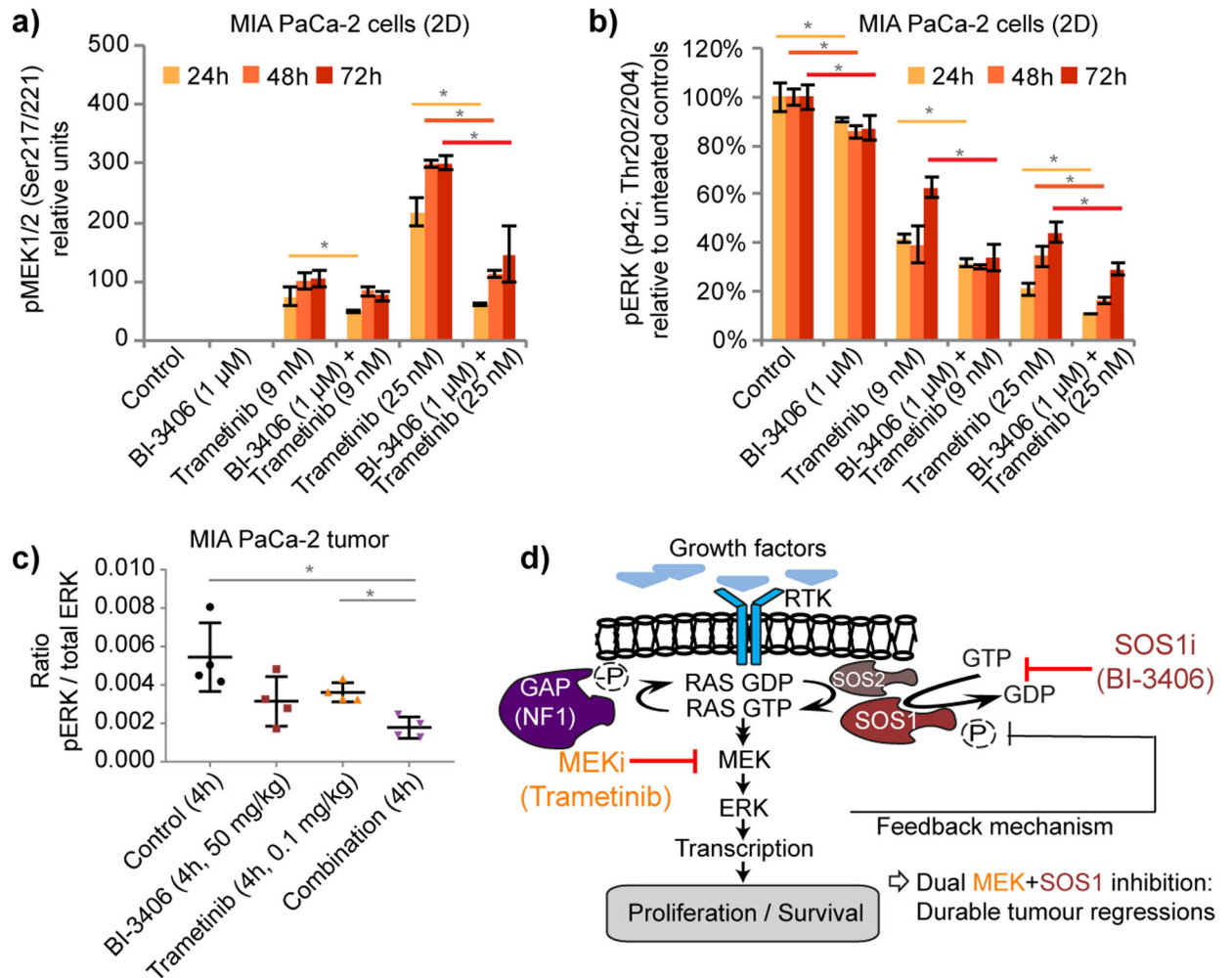
Figure 5: Biomarker modulation upon combined SOS1 and MEK inhibition

a, Western blot analysis of pMEK1/2 in MIA PaCa-2 cells grown in vitro in 2D and treated with BI-3406, trametinib, or the combination for the indicated time periods (n=3, means ±s.e.m.). **b,** Western blot analysis of pERK in MIA PaCa-2 cells grown in vitro in 2D as in a; (a and b, one tailed t-test p=0.05; two-tailed t-test: p=0.1). **c,** Multiplexed immunoassay measurements of pERK and total ERK in MIA PaCa-2 tumor xenografts at 4 h post-treatment (n=4 animals per group, means±s.d.; two tailed t-test). **d,** Proposed model of the effects of combined MEK and SOS1 inhibition. Inhibition of MEK results in the attenuation of negative feedback control leading to increased SOS1 activity KRAS-GTP loading driving reactivation of downstream signals. Based on these adaptive responses, effects of MEK inhibitors on cell proliferation and survival are limited. Adaptive responses can be abrogated through combined blockade of MEK and SOS1, which prevents MEK inhibitor-induced KRAS-GTP loading and reduces signaling downstream of KRAS, resulting in durable tumor regressions.